Journal of
Synchrotron
Radiation

ISSN 0909-0495

Received 27 June 2005
Accepted 31 October 2005

The new diffractometer for surface X-ray diffraction at beamline BL9 of DELTA

Christof Krywka,[a]* Michael Paulus,[a] Christian Sternemann,[a] Martin Volmer,[a] Arndt Remhof,[b] Gregor Nowak,[b] Alexei Nefedov,[b] Birgit Pöter,[c] Michael Spiegel[c] and Metin Tolan[a]

[a]Institute of Physics/DELTA, University of Dortmund, D-44221 Dortmund, Germany, [b]Institute of Physics, University of Bochum, D-44780 Bochum, Germany, and [c]Max-Planck-Institut für Eisenforschung, D-40237 Düsseldorf, Germany. E-mail: christof.krywka@uni-dortmund.de

The experimental endstation of the hard X-ray beamline BL9 of the Dortmund Electron Accelerator is equipped with a Huber six-circle diffractometer. It is dedicated to grazing-incidence X-ray diffraction and X-ray reflectivity experiments on solid surfaces and thin films as well as to powder diffraction measurements. A new set-up for grazing-incidence X-ray scattering of liquids has been built up using a silicon mirror to reflect the incident X-ray to the liquid surface at angles of incidence around the critical angle of total reflection of the sample. X-ray reflectivity measurements of a polymer film and grazing-incidence X-ray diffraction measurements of an epitaxically grown $Gd_{40}Y_{60}$ film, an oxidized surface of Fe-15at.%Al alloy and aqueous salt solutions are presented and discussed.

© 2006 International Union of Crystallography
Printed in Great Britain – all rights reserved

Keywords: X-ray scattering; grazing-incidence diffraction; X-ray reflectivity; liquid surfaces; structure factor; GID; GISAXS.

1. Introduction

The design of materials with specific electronic, magnetic, optical or mechanical properties draws increasing attention to methods that allow the characterization of solid and thin-film layered surfaces. In particular, grazing-incidence X-ray diffraction (GID) and X-ray reflectivity (XRR) measurements have become invaluable tools for probing a variety of sample systems whose surface and near-surface structures remain inaccessible to other techniques (Rauscher *et al.*, 1999; Stangl *et al.*, 2000). The penetration depth in an X-ray grazing-incidence experiment can be easily controlled as a function of the angle of incidence, hence different sensitivity of the experiment with respect to bulk and surface signal is obtained. This allows the analysis of morphology and roughness of surfaces or unexposed interfaces in a single set-up (Gibaud & Hazra, 2000). Average parameters for the size, shape and distribution of macroscopic or microscopic structures are accessible in a GID experiment. Moreover, capillary-wave-induced surface roughness is observable in such measurements as a function of the surface tension of a fluid. Furthermore, time-resolved and *in situ* control of growth processes in ultrahigh-vacuum or high-pressure gases allow features mentioned above to be monitored, along with other parameters, *e.g.* crystallization defects, that are relevant in a production or design process (see *e.g.* Gibaud *et al.*, 2004; Revenant *et al.*, 2004). Information about the film thickness, the surface and interfacial roughnesses and the electron density profile perpendicular to the film plane can be obtained with angstrom resolution *via* XRR experiments [an overview is given by *e.g.* Tolan (1999)].

Recently, a set-up for X-ray reflectivity and grazing-incidence X-ray diffraction was built at beamline BL9 of the Dortmund Electron Accelerator (DELTA). This set-up will be discussed within this article along with some key applications of X-ray surface diffraction. The outline of the paper is as follows. In the next section a short overview of possible experimental configurations of the endstation at beamline BL9 is presented. In §3 the experimental set-up for grazing-incidence X-ray diffraction on solids and thin liquid films is described, together with the set-up for the study of liquid surfaces. First X-ray reflectivity and grazing-incidence diffraction measurements on solids and liquids are presented and discussed in §4. Finally, conclusions and a short outlook are given in §5.

2. Endstation at beamline BL9 of DELTA

DELTA is a synchrotron radiation source located at the University of Dortmund, Germany (Tolan *et al.*, 2003). The storage ring is operated at a maximum energy of 1.5 GeV with a typical electron beam current of 120 mA and lifetimes of about 10 h. Synchrotron radiation is produced by several dipole magnets, two undulators and a superconducting asymmetric wiggler (SAW), where three beamlines (BL8–10) are attached to the SAW outlet chamber. At beamline BL9 the incident radiation is monochromated by means of a Si(311)

double-crystal monochromator which provides an energy resolution of $\Delta E/E \simeq 10^{-4}$. The sagittally bent second monochromator crystal allows for horizontal focusing at the sample position. The monochromator provides synchrotron radiation in an energy range between 4 keV and 30 keV. For a more detailed description, see Paulus *et al.* (2005). Grazing-incidence X-ray diffraction and X-ray reflectivity experiments on solid surfaces and thin liquid films can be performed using the standard set-up of the six-circle diffractometer described in §3.1. Utilizing a silicon mirror this set-up can be applied to perform measurements on liquid samples as will be discussed in §3.2. Furthermore, the diffractometer can be used for X-ray powder diffraction experiments (see *e.g.* Weber *et al.*, 2005). In addition, the beamline is equipped with a spectrometer in Rowland geometry for resonant and non-resonant inelastic X-ray scattering experiments (see *e.g.* Sternemann *et al.*, 2003; Enkisch *et al.*, 2004). Moreover, energy-dispersive X-ray fluorescence analysis with a spatial resolution of about 10 μm (von Bohlen *et al.*, 2005) and X-ray standing-wave measurements are possible.

3. Experimental set-up for surface X-ray diffraction

3.1. Solid surfaces and thin liquid films

The schematic experimental set-up for GID and XRR measurements at BL9 of DELTA is shown in Fig. 1. The incident beam is collimated by two slit systems (S3, S4). In between these slit systems, several absorber foils are available to attenuate the X-ray beam. The intensity of the incident beam is monitored by NaI detectors (detector 1 and 2) located in front of and behind the absorber.

The scattered radiation is detected by another NaI detector (detector 3). The slit S5 reduces background radiation and the detector slit S6 determines the angular resolution in a diffraction experiment. The distance between sample and detector 3 is 1 m. Within this scattering geometry the size of the X-ray beam is approximately 1 mm horizontally and 0.1–3 mm vertically.

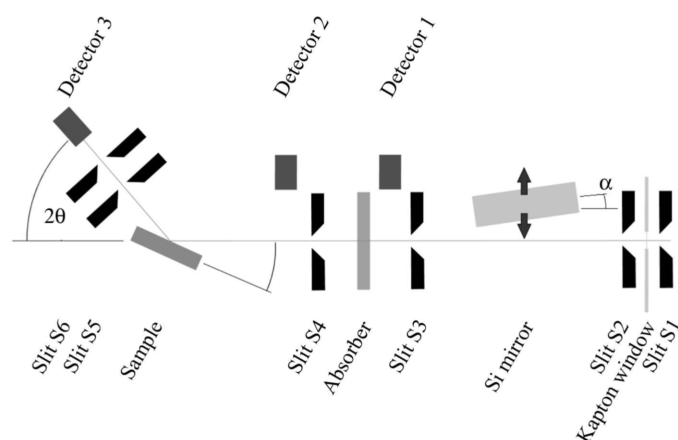

Figure 1
Scheme of the experimental set-up for X-ray reflectivity and diffraction measurements at BL9 of DELTA.

Diffraction and reflectivity scans are carried out in vertical scattering geometry using Θ' and Θ together with $\Theta' = 2\Theta$, respectively (see Fig. 2). In order to establish a horizontal scattering geometry the diffractometer can be rotated in Ψ. Moreover, it can be translated in x, y and z directions. Ψ scans are limited by the set-up to angles below 40°. Experiments can be performed both in in-plane and out-of-plane geometry without changing the set-up by rotating the χ-circle of the Eulerian cradle by 90°. In case of bulky and heavy sample environments a separate alignment stage is available so that the Eulerian cradle of the diffractometer has not to be used. The silicon mirror with its tilt angle α shown in Fig. 1 is necessary for performing experiments on liquid surfaces, as will be discussed in the following section. The slit systems S1 and S2 determine the beam position with respect to the mirror. They are also used together with the Rowland spectrometer set-up.

3.2. Liquids

The GID experiments on solid surfaces and thin liquid films require the sample to be tilted around an axis perpendicular to the direction of the incident photon beam. This is not possible in the case of a liquid sample. Here the incident beam has to be bent from its original direction towards the horizontally leveled surface which is an inherent feature of a liquid sample. If the critical angle of total reflection of the liquid sample is in the vicinity of 0.05–0.15° a polished silicon mirror can be used to reflect the incident photon beam to the sample surface. The mirror installed at BL9 is a silicon rod with an evenly polished surface of size 140 mm × 25 mm (Seeck *et al.*, 2003). Its layout is shown in Fig. 3 along with that of the mirror holder.

The mirror was commissioned at an incident energy of 13 keV. Higher harmonics of the monochromator were efficiently suppressed by the silicon mirror as its reflectivity drops drastically with increasing energy. A reflectivity of about 74% was achieved with the mirror tilted by 0.075° resulting in a total deflection angle of 0.15° at the sample surface. At this

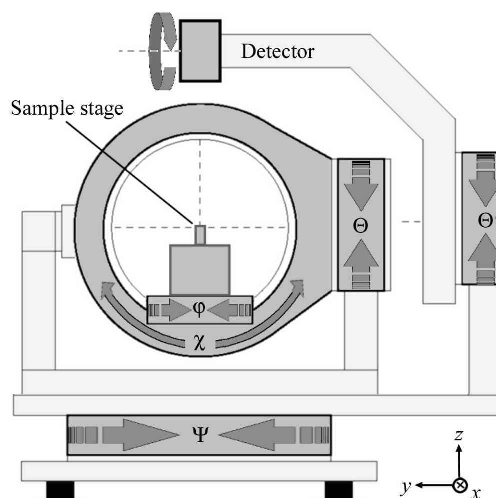

Figure 2
Sketch of the diffractometer indicating the translation and rotation axes (see text for detailed information).

angle the mirror's acceptance with respect to the incident beam height is 0.32 mm. Small deviations from an ideally flat mirror surface cause a decrease of the reflected intensity. These deformations can be corrected by a set of screws embedded into the mirror housing (see Fig. 3). The mirror has an H-shaped profile to be fixed free of tension by a line of screws that sink into the mirror's side grooves. Fine tunable pressure can then be applied to the opposite side of the reflecting surface by means of another series of screws in the mirror housing which is movable and tiltable in all directions. Apart from correcting the mirror deficiencies it is possible to bend the mirror into a slight concave shape, so that vertical focusing of the reflected photon beam is obtained. In this manner the height of the reflected beam could be reduced to about 0.1 mm FWHM (full width at half-maximum). The profiles of the direct and the reflected vertically focused beam were measured by scanning the vertical slit position of S4, and are shown in Fig. 4. The photon intensity per area (shaded part of the reflected beam in Fig. 4) increases by 47%. The focusing has been tested to work at different angles and incident photon energies yielding similar results.

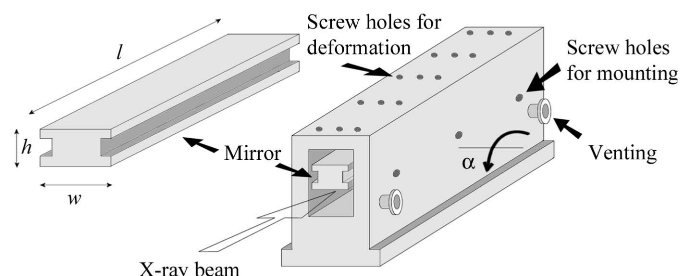

Figure 3
Layout of the mirror for the liquid sample set-up. The Si mirror is fixed with its polished side down by means of six screws alongside the groove. Any deformation of the mirror is performed by adjusting the set of screws placed in the mirror mounting top side. The tilt angle α can be adjusted *via* a two-circle goniometer onto which the mirror housing is mounted. The mirror can be tilted around an axis parallel to the beam direction and translated in all directions. The mirror dimensions are w = 25 mm, h = 10 mm, l = 140 mm.

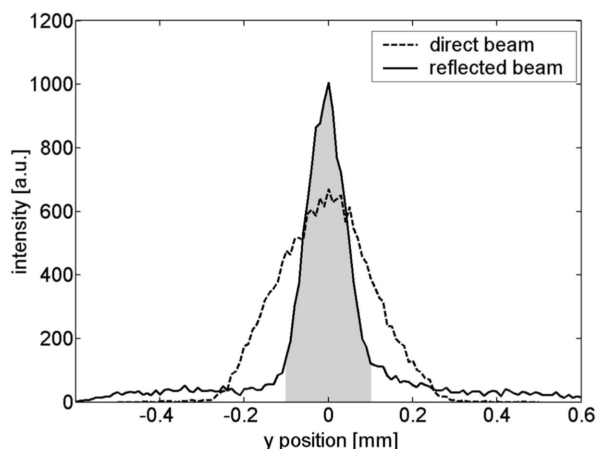

Figure 4
Vertical profile of the direct and reflected X-ray beam measured by a vertical scan of the S4 slit position.

The sample cell for measurements on liquids is optimized with respect to sample size and air scattering. The liquid sample can be filled into a shallow steel plate so that a liquid surface of 20 cm in diameter is obtained. A controlled water-saturated helium atmosphere prevents a drift of the surface position owing to evaporation and significantly reduces air scattering. The cell is mounted within the Eulerian cradle. Utilizing the silicon mirror, a fixed angle of incidence can be chosen. X-ray diffuse scattering on liquids can be measured by scanning the angles Ψ or Θ'. Because the angle of incidence is limited by the critical angle of total reflection of Si, conventional X-ray reflectivity measurements on liquid surfaces are not possible.

4. First test experiments

4.1. X-ray reflectivity

Measurements of X-ray reflectivities on thin films have been performed at an incident energy of 13 keV using a beam size of 1 mm $\times$ 0.2 mm (horizontal $\times$ vertical) utilizing the diffractometer set-up described in §3.1. As an example, the reflectivity curve of a tempered polystyrene film on a 10 mm $\times$ 10 mm Si wafer is presented in Fig. 5 on a logarithmic intensity scale. The momentum transfer q_z is given by $q_z = (4\pi/\lambda)\sin(\Theta)$ where λ is the wavelength of the incident beam and Θ is the glancing angle.

The background was measured separately by a longitudinal diffuse scan with a constant angular detector offset of 0.1° from the specular condition. This reflectivity measurement was corrected for this background. The X-ray reflectivity of the polystyrene film was fitted on the basis of the well known Parratt algorithm (Parratt, 1954), modified according to Névot & Croce (1980) taking roughnesses into account; it is defined as the root-mean-square of the electron density height fluctuation at the interface. The corresponding fit function is shown in Fig. 5 (solid line). As a result, a layer thickness of 134.5 $\pm$ 2 Å and a surface roughness of 6 $\pm$ 1 Å were obtained for the polystyrene film with a density of 1.04 g cm^{-3}. These

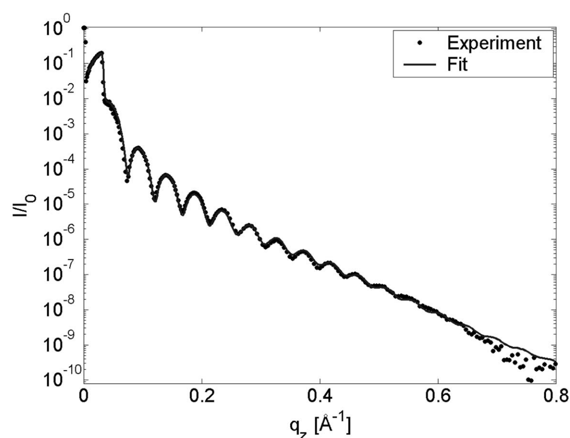

Figure 5
Experimental X-ray reflectivity of a polystyrene film on a Si wafer (dots) compared with the result of a fit on the basis of the Parratt algorithm (solid line).

values are in good agreement with results of reference measurements on this sample. Overall, a dynamic range of nine orders of magnitude is obtained.

4.2. Characterization of epitaxically grown metal films

The structural characterization of thin metal films is necessary for the understanding of magnetic and electronic properties of these systems. The structural key parameters are the surface roughness and film thickness, the lattice parameters and coherence lengths (in-plane and out-of-plane with respect to the sample surface) as well as the epitaxic relation of the crystal structures of the film and the substrate. Results of measurements on a $Gd_{40}Y_{60}$ film grown on a Nb(110)/Al_2O_3 (11–20) substrate are presented as an example of a standard structural characterization. In Fig. 6 a high-angle radial scan ($\Theta - 2\Theta$ scan, out-of-plane) aligned with respect to the Gd/Y (0001) planes is presented. From small to high angles the GdY (0002), Al_2O_3 (11–20) and Nb (110) Bragg reflections appear and confirm parallel growth of the respective lattice planes. The Nb (110) reflection is accompanied by a series of diffraction maxima marked by the arrows in Fig. 6. Analogous to the diffraction fringes in the small-angle reflectivity regime, they originate from the finite size of the Nb layer. These finite-size oscillations would be more obvious also for small Bragg angles by using a weaker absorber foil for the incident beam. A detailed analysis of the GdY (0002) reflection yields a coherence length of about 200 nm, which corresponds to the film thickness determined by X-ray reflectivity measurements.

It should be noted that out-of-plane radial scans only probe the coherence length normal to the film plane. Therefore, information about the in-plane structure cannot be obtained from this scan. In analogy to the previous paragraph, we have measured the in-plane coherence length and the crystal orientation in the surface scattering configuration. In these measurements the angle of incidence was kept constant and equal to the critical angle for the total external reflection from GdY alloy.

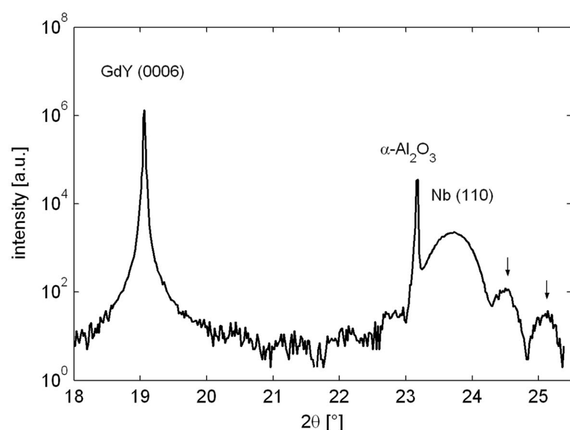

Figure 6
Out-of-plane high-angle radial scan ($\Theta - 2\Theta$ scan) of an epitaxically grown $Gd_{40}Y_{60}$ film on a Nb (110)/Al_2O_3 (11–20) substrate. Finite-size oscillations of the Nb (110) reflection are indicated by arrows.

Fig. 7(*a*) shows a part of an ω-scan where the sample is rotated around the film normal and the detector is kept fixed at the GdY (11–20) Bragg position. Reflections are separated by 60° in accordance with sixfold symmetry. The varying intensity is caused by slight misalignment of the sample. An in-plane radial scan is shown in Fig. 7(*b*) for the GdY (11–20) reflection. A coherence length of 22.7 nm is obtained from this scan which is a typical value for rare-earth metallic films grown on single-crystalline Nb buffers. These measurements clearly demonstrate the feasibility of the set-up discussed in §3.1 to study the structural properties of epitaxically grown films.

4.3. Characterization of the surface oxidation on Fe–Al alloys

The phase composition of oxide layers grown on Fe–Al alloy samples as a function of different heat treatment is of special interest for high-temperature applications in oxidizing and sulphidizing environments (see *e.g.* Klöwer, 1997). These oxide layers are only several hundreds of nm thick. Characterization methods that apply surface-sensitive techniques are therefore necessary. XPS (X-ray photoelectron spectroscopy) experiments yield information about the layer thickness but information about the crystallographic phase composition is not accessible (Shankar Rao *et al.*, 2003). Thus

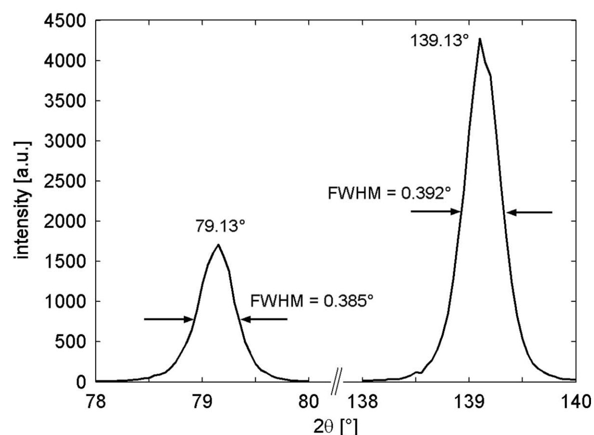

(*a*)

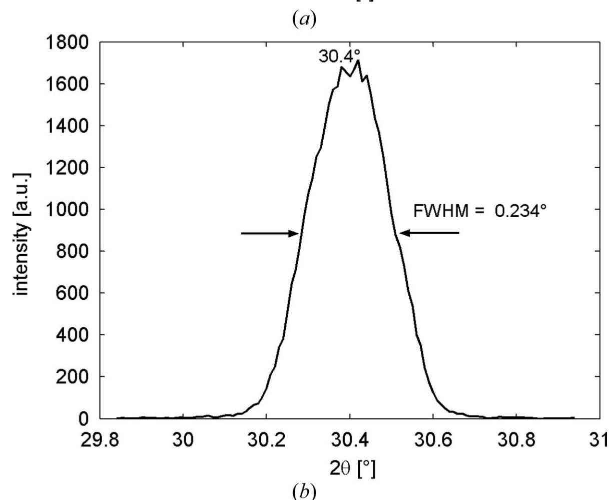

(*b*)

Figure 7
(*a*) ω-scan of the GdY (11–20) Bragg reflection at $2\Theta = 30.4°$. (*b*) In-plane radial scan ($\Theta - 2\Theta$-scan) of the GdY (11–20) reflection.

measurements on Fe-15at.%Al alloy with grazing-incidence X-ray diffraction have been carried out. The Fe-15at.%Al sample of 10 mm × 10 mm × 1 mm was cut by spark erosion from cast material, ground and polished. Oxidation was performed in a horizontal tube furnace for 5 h at a temperature of 973 K in dry synthetic air (20 vol.% O_2 and 80 vol.% N_2) under atmospheric pressure. After preparation the sample was kept in a desiccator in order to prevent changes of the formed oxide scale.

Using XPS, two oxide layers could be identified indicating a double oxide layer scale. This scale consists of an outer 60 nm-thick layer of Fe_2O_3 and Al_2O_3 followed by an inner layer of pure Al_2O_3 of thickness 60 nm. A diffraction pattern of this sample was measured at an incident photon energy of 13 keV and an angle of incidence of 0.27°. Under these conditions the penetration depth of the X-rays is about 700 nm assuming a density of 4.77 g cm^{-3} for the mixed oxide scale. The X-ray diffractogram shown in Fig. 8 clearly indicates contributions from the bulk material α-Fe but also from the oxide layers which consist of hematite (Fe_2O_3) and corundum (α-Al_2O_3). Other polymorphs of Al_2O_3, like γ-Al_2O_3 or Θ-Al_2O_3, were expected but could not be detected in the surface oxide layer of this sample. The absence of these polymorphs in the oxide layer caused by the special heat treatment of the sample is of advantage for high-temperature applications because aluminium and oxygen diffuse faster within the polymorphs than in α-Al_2O_3 leading to higher oxidation rates and less corrosion resistance (Grabke, 1999). A strong signal of Fe_2O_3 and α-Al_2O_3 from thin layers of thickness 60 nm could be clearly resolved under these experimental conditions. Hence, the applicability of surface-sensitive X-ray diffraction at grazing incidence for analysis of phase composition of surface oxide layers is demonstrated. Moreover, depth-resolved X-ray diffraction experiments can be accomplished by variation of the angle of incidence.

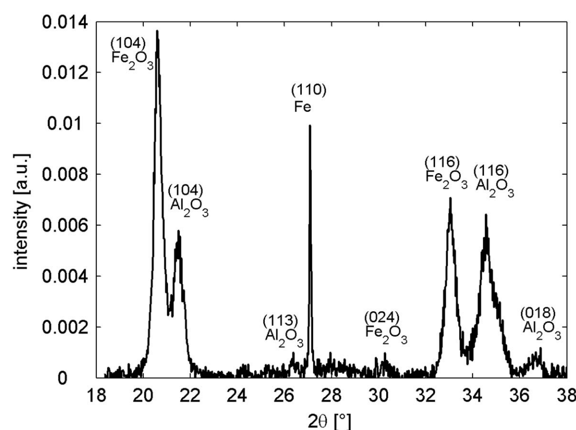

Figure 8
Grazing-incidence X-ray diffractogram measured at 13 keV with an angle of incidence of 0.27° for a Fe-15at.%Al sample oxidized at 973 K for 5 h in dry synthetic air. The Bragg reflections are assigned to the bulk material α-Fe, the oxide layers Fe_2O_3 and α-Al_2O_3.

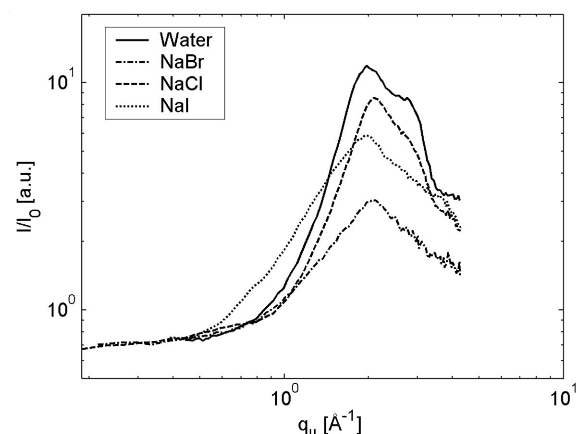

Figure 9
Structure factor of water and aqueous salt solution (5 mol l^{-1}) measured at a grazing angle of 0.22° at 15.2 keV.

4.4. Structure factor of aqueous salt solutions

The bulk structure factors of pure water and five molar aqueous solutions of NaBr, NCl and NaI salts were measured in surface-scattering geometry in order to test the mirror set-up at an incident photon energy of 15.2 keV. The angle of incidence was set to 2α = 0.22°, utilizing the silicon mirror set-up described above, thus being higher than the critical angle of total reflection of water at 0.095°. The diffractometer angle Ψ was scanned from 0° to 34° at $\Theta' = 2\alpha$ which corresponds to a maximum wavevector transfer $q_{||}$ parallel to the sample surface of 4.5 $\mathring{A}^{-1}$ with $\mathbf{q} = (q_x, q_y, 0)^{\rm T} = (2\pi/\lambda) \times [\cos(\Theta')\cos(\Psi) - \cos(2\alpha), \cos(2\alpha)\sin(\Psi), 0]^{\rm T}$. The measured intensity was normalized to the signal of a NaI monitor detector located in front of the sample cell.

The experimental results are presented in Fig. 9. The structure factor of pure water is found to be in good agreement with measurements of Fradin *et al.* (2000). The double-peaked structure of the water structure factor is discussed in detail by Barker *et al.* (2000) using molecular dynamics calculations. Comparison of the structure factor of the pure solvent with that of aqueous salt solutions indicates the contribution of the solute to the scattering signal. While the main peak of the water structure factor remains dominant in each case, its shoulder for higher $q_{||}$ becomes less distinctive in the spectra of the solutions. Also an additional structure is visible at lower $q_{||}$ corresponding to the mean distance of solved salt ions.

5. Conclusion and outlook

Grazing-incidence X-ray diffraction represents a valuable approach for probing the surface and near-surface structure of solid and in particular soft or liquid systems. The beamline was successfully adapted for measurements on both solid and liquid surfaces by building up a silicon mirror system utilizing total external reflection for deflecting the incident beam onto the sample surface. The focusing properties of the mirror effectively allow an increase of flux per area at the sample position, while the vertical beam height is simultaneously reduced to about 0.1 mm. Grazing-incidence measurements were performed on water and aqueous solutions of sodium

salts yielding their concentration-dependent structure factors. X-ray reflectivities were taken on a well examined reference layer system where the estimated layer thickness, roughness and density are found to be in accordance with reference measurements. A dynamic range of nine orders of magnitude can be used for the analysis of X-ray reflectivity data. Moreover, a full structural characterization of epitaxically grown metal films was performed and the surface roughness, film thickness, lattice parameters, coherence lengths and the epitaxic relations were determined. The phase composition of a thin surface layer of an oxidized Fe–Al alloy was exemplarily estimated *via* recording diffraction patterns in surface-sensitive geometry. Hence, the versatile applications demonstrate the ability to fully characterize surface and near-surface structures utilizing the six-circle diffractometer at BL9 of DELTA. The set-up will be further extended by a two-dimensional MAR image-plate detector allowing X-ray diffraction with texture analysis and small-angle X-ray scattering, whereas the latter is of special interest for the study of biophysical processes, *e.g.* the folding of protein macromolecules.

The authors would like to thank O. H. Seeck and R. Nowak of HASYLAB (Hamburger Synchrotron Strahlungslabor, Hamburg, Germany) for technical support, supply of the silicon mirror and helpful discussions during the realization of the mirror set-up. We would like to acknowledge M. Krämer for providing the polymer sample. M. Paulus is grateful for the financial support by the Graduiertenkolleg 'Struktur und Dynamik Beziehungen in mikrostrukturierten Systemen' at the University of Dortmund. The authors thank the DELTA machine group for providing the synchrotron radiation and technical support.

References

Barker, D. R., Wilson, M., Madden, P. A., Medvedev, N. N. & Geiger, A. (2000). *Phys. Rev. E*, **62**, 1427–1430.

Bohlen, A. von, Hergenröder, R., Sternemann, C., Paulus, M., Radtke, M. & Riesemeier, H. (2005). *Instrum. Sci. Technol.* **33**, 137–150.

Enkisch, H., Sternemann, C., Paulus, M., Volmer, M. & Schülke, W. (2004). *Phys. Rev. A*, **70**, 022508.

Fradin, C., Braslau, A., Luzet, D., Smilgies, D., Alba, M., Boudet, N., Mecke, K. & Daillant, J. (2000). *Nature (London)*, **403**, 871–874.

Gibaud, A., Dourdain, S., Gang, O. & Ocko, B. (2004). *Phys. Rev. B*, **70**, 161403.

Gibaud, A. & Hazra, S. (2000). *Curr. Sci.* **78**, 1467–1477.

Grabke, H. J. (1999). *Intermetallics*, **7**, 1153–1158.

Klöwer, J. (1997). *Oxidation of Intermetallics*, p. 203. Weinheim: Wiley-VCH.

Névot, L. & Croce, P. (1980). *Rev. Phys. Appl.* **15**, 761–779.

Parratt, L. G. (1954). *Phys. Rev.* **95**, 359–369.

Paulus, M., Fendt, R., Sternemann, C., Gutt, C., Hövel, H., Volmer, M., Tolan, M. & Wille, K. (2005). *J. Synchrotron Rad.* **12**, 246–250.

Rauscher, M., Paniago, R., Metzger, H., Kovats, Z., Domke, J., Peisl, J., Pfannes, H. D., Schulze, J. & Eisele, I. (1999). *J. App. Phys.* **86**, 6763–6769.

Revenant, C., Leroy, F., Lazzari, R., Renaud, G. & Henry, C. R. (2004). *Phys. Rev. B*, **69**, 035411.

Seeck, O. H., Nowak, R., Maul, U., Wengler, R., Kracht, Th. & Brüggemann, U. (2003). *HASYLAB Annual Report.* HASYLAB, Hamburg, Germany.

Shankar Rao, V., Norell, M. & Raja, V. S. (2003). *Corr. Sci.* **45**, 2717–2728.

Stangl, J., Holy, V., Roch, T., Daniel, A., Bauer, G., Zhu, J., Brunner, K. & Abstreiter, G. (2000). *Phys. Rev. B*, **62**, 7229–7236.

Sternemann, C., Volmer, M., Soininen, J. A., Nagasawa, H., Paulus, M., Enkisch, H., Schmidt, G., Tolan, M. & Schülke, W. (2003). *Phys. Rev. B*, **68**, 035111.

Tolan, M. (1999). *X-ray Scattering from Soft-Matter Thin Films.* Berlin: Springer.

Tolan, M., Weis, T., Wille, K. & Westphal, C. (2003). *Synchrotron Rad. News*, **16**, 9–11.

Weber, H.-J., Keller, H. L., Paulus, M. & Sternemann, C. (2005). *Phys. Rev. B*, **72**, 045432.